



저작자표시-비영리-변경금지 2.0 대한민국

이용자는 아래의 조건을 따르는 경우에 한하여 자유롭게

- 이 저작물을 복제, 배포, 전송, 전시, 공연 및 방송할 수 있습니다.

다음과 같은 조건을 따라야 합니다:



저작자표시. 귀하는 원저작자를 표시하여야 합니다.



비영리. 귀하는 이 저작물을 영리 목적으로 이용할 수 없습니다.




변경금지. 귀하는 이 저작물을 개작, 변형 또는 가공할 수 없습니다.

- 귀하는, 이 저작물의 재이용이나 배포의 경우, 이 저작물에 적용된 이용허락조건을 명확하게 나타내어야 합니다.
- 저작권자로부터 별도의 허가를 받으면 이러한 조건들은 적용되지 않습니다.

저작권법에 따른 이용자의 권리는 위의 내용에 의하여 영향을 받지 않습니다.

이것은 [이용허락규약\(Legal Code\)](#)을 이해하기 쉽게 요약한 것입니다.

[Disclaimer](#) 

Virtual Sensing for Structural Health Monitoring of Off-shore Structures

Rajendra Prasath Palanisamy

Department of Urban and Environmental Engineering
(Urban Infrastructure Engineering)

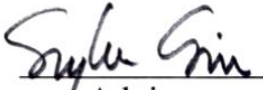
Graduate School of UNIST

Virtual Sensing for Structural Health Monitoring of Off-shore Structures

A thesis/dissertation
submitted to the Graduate School of UNIST
in partial fulfillment of the
requirements for the degree of
Master of Science

Rajendra Prasath Palanisamy

12.09.2015
Approved by


Advisor
Sung-Han Sim

Virtual Sensing for Structural Health Monitoring of Off-shore Structures

Rajendra Prasath Palanisamy

This certifies that the thesis/dissertation of Rajendra Prasath Palanisamy is
approved.

12.09.2015



Advisor: Dr. Sung-Han Sim



Thesis Committee Member: Dr. Marco Torbol



Thesis Committee Member: Dr. Young Joo Lee

Abstract

Offshore structures are generally subjected to harsh environment with strong tidal current and wind loading, which demands robust and reliable Structural Health Monitoring (SHM) to avoid any catastrophic failure. The growing size, complexity, and harsh environment of offshore structures lead to difficulties in sensor deployment and maintenance. Response at critical locations in complex offshore rigs are inaccessible during sensor deployment. Moreover, their operational environment demands frequent sensor maintenance for uninterrupted monitoring. Virtual sensing addresses these issues by estimating unmeasured responses with the help of measured responses. This dissertation delineates a virtual sensing method based on Kalman state estimator to combine multi-sensor data under non-stationary random excitation. The estimation algorithm effectively uses the FE model of a structure to predict and fuse different type of structural response (acceleration, strain, and angular displacement). This study investigates various combinations of sensor fusion to improve the estimation accuracy. In addition, an erroneous model is purposefully used to support the robustness and practicality of estimator. The performance of virtual sensing is successfully verified with numerical and experimental test over simply-supported and bottom fixed off-shore structure. Test results conclude that the unmeasured responses are reasonably recovered from measured responses.

Contents

I.	INTRODUCTION	1
II.	BACKGROUND STUDY	4
	2.1 SHM in offshore structures.....	4
	2.2 Virtual sensing.....	4
	2.3 Kalman filter.....	5
	2.3.1 Random variables.....	5
	2.3.2 Kalman filter (state estimator).....	6
III.	DATA FUSION APPROACH FOR NON-STATIONARY RANDOM INPUTS	9
IV.	NUMERICAL AND EXPERIMENTAL VALIDATION	13
	4.1 Validation with simply supported beam.....	13
	4.1.1 Numerical validation.....	13
	4.1.2 Experimental validation.....	18
	4.2 Validation with model of bottom fixed offshore structure.....	22
	4.2.1 Numerical validation.....	22
	4.2.2 Experimental validation.....	27
V.	CONCLUSION, LIMITATION AND FUTURE SCOPE	33
VI.	REFERENCES	35
VII.	ACKNOWLEDGEMENT	37

Chapter 1

INTRODUCTION

Bottom-fixed offshore structures such as mono-piles, tripods, jackets, and gravity-based structures, have been widely utilized for the purpose of extracting oil and gas, supporting metrological towers and multi-purpose ocean science platforms. They are expanding their applications for supporting ocean energy facilities including offshore wind turbines and tidal stream turbines. Indeed, the number of bottom-fixed offshore structures has been rapidly increased for the recent several years as the increase of the large-scale offshore wind farms. As these offshore structures are generally built in harsh environment with strong wind and tidal current that can expedite structural degradation and potentially cause critical damages. In addition, the quasi-periodic excitation forces due to the rotating devices including rotor, main shaft, and generators, can be a source of fatigue issues. Being more prone to structural failures due to the various external excitations, these offshore structures for OEFs are carefully maintained to prevent catastrophic collapses and prolong the lifetime.

SHM provides an effective means for the appropriate maintenance of the offshore structures to assess the current status as well as the remaining lifetime. SHM is typically performed by collecting measured response data at the limited number of accessible locations using sensors such as accelerometers and strain-gauges [1]. In monitoring offshore structures for OEFs, most of the fatigue-sensitive spots and critical members are located in inaccessible regions for direct measurements (e.g., at the mudline several meters below the water level). Thus, the sensor installation can be quite challenging for those important regions deep in the water. Moreover due to harsh environment, the sensors deployed in those critical locations are prone to damage.

Monitoring fatigue is important for sustainable usage of off-shore structure. Accurate fatigue assessment is based on stress response time histories. Strain measurements are generally employed to obtain the stress time histories. In cases of complex offshore structures, strain measurements at several expected critical locations are required, it is practically and economically challenging to install strain gauges at all required locations. Thus, only limited physical sensor distribution is possible and a virtual sensing technique is required to obtain strain time history at other critical location.

Recently, virtual sensing approaches are being actively developed to indirectly obtain responses at unmeasured locations. Various efforts for virtual sensing has been made such as finite element model

updating with modal expansion [2], natural input modal analysis [3], time varying auto-regressive model [4], and the model-based Kalman state estimator. Among these efforts, the Kalman state estimator associated with the FE model has been known as an effective tool to estimate the unmeasured responses. Papadimitriou et al. (2009) [5] used limited strain measurements in the numerical simulation to obtain strain in the entire body, which is subsequently utilized to estimate fatigue remaining life of the structural model. Smyth and Wu (2007) [6] used the Kalman filter to fuse acceleration and displacement with different sampling rates to produce more accurate displacements. Based on the idea that multi-sensor data has the potential to improve the performance of response estimation [7], [8], [9], and [10]. Jo and Spencer (2014) [11] numerically verified that the combination of acceleration and strain in conjunction with the Kalman filter better estimates unmeasured strains compared to the sole use of acceleration or strain. Yet, the virtual sensing using the model-based Kalman filter with multi-sensor data has not been fully explored but limited to ideal numerical simulations with analytical FE models, the sole combination of acceleration and strain, and non-stationary random inputs.

Followed by exploring the possibilities of virtual sensing, the model-based virtual sensing technology has been adopted for SHM of off-shore structures. Iliopoulos et al. (2014) [2] proposed response estimation techniques using a modal decomposition and expansion algorithm and validated the performance of their method using measurement data obtained from a monitoring campaign on an offshore Vestas V90 3 MW wind turbine on a monopile foundation. This study is limited to zero mean responses. Van der Male and Lourens (2014) [12] proposed a strategy to monitor the accumulated fatigue damage in real-time, employing a joint input-state estimation algorithm. Measuring the operational vibrations at well-chosen locations enables the estimation of strain responses at unmeasured locations. The estimation algorithm is applied to a wind turbine on a lattice support structure, for which the response estimates of the lattice members are based on measurements on the turbine tower only. Their algorithm is verified only with the numerically simulated responses, while experimental results have not been reported in public domain.

This study investigates a virtual sensing strategy based on the Kalman filtering associated with the finite element model tailored to the offshore structures under non-zero mean stochastic external loads. The multi-metric sensor data fusion technique is recently highlighted to overcome the difficulties related to the non-zero mean static response estimation from acceleration responses by means of fusion of sensors good for low frequency region and high frequency region such as strain and acceleration or inclination and acceleration and so on. The strain response of bottom-fixed offshore structures for OEFs consists of high level of strain responses due to mean thrust force and also high level of dynamic excitations from the turbulent effect and periodic operational loads from rotors. Therefore it is very difficult to extract accurate

responses from homogeneous sensor networks such as acceleration sensors network or strain sensors network. Hence the multi-metric sensor network is utilized and the signal processing are carried out based on the Kalman filtering to estimate the responses at unmeasured locations by incorporating the finite element model. The proposed method is numerically and experimentally verified using a simply supported beam and a four-leg portal frame in a circulating water channel.

Chapter 2

BACKGROUND STUDY

This chapter covers basic studies about SHM, random variables and Kalman filter. First section of this chapter illustrates the importance of health monitoring of off-shore structures. Followed by, importance of virtual sensing and how Kalman filter is used in virtual sensing. Finally, the data fusion technique employed to enhance the accuracy of virtual sensing is discussed.

2.1 SHM in offshore structures

SHM and damage detection techniques are widely used in the field of civil, offshore, wind turbine structures to reduce renovation costs, increase operational lifetime, and to prevent catastrophic failure [1]. Structural health monitoring is emerging with its application in both newly built complex structures to aging structures. Early research in SHM is about monitoring change in modal properties viz., Natural frequency and mode shape, before and after damage. This technique is still used for SHM of various structures, but recent developments in computing techniques made complex signal processing algorithms possible. Such examples are Monte Carlo simulation [13], Kalman Filter [14], Extended Kalman Filter [15], Uncented Kalman filter [16], etc.

The application of SHM on offshore structures is important, as these structures are the large value to the economy and built in harsh environment. Typically offshore structures are subjected to strong wind and tidal current which provide them a harsh environment. In addition to this loading, sea water leads to material degradation and lack of strong foundation may lead to failure. Moreover, offshore structures being built on oceans, makes them inaccessible to maintain and retrofit frequently. Thus Structural health monitoring in offshore structures are ineluctable.

2.2 Virtual sensing

As the location of offshore structures are not easily accessible for maintenance, SHM system for offshore structures should be more reliable and robust. Virtual sensing improves the robustness of SHM system. Virtual sensing or proxy sensing shall be defined as, estimation of unmeasured responses with available measurements. In conventional SHM system, when a sensor is damaged or malfunctions the whole system stops and can be operational only when the sensors is replaced or retrofitted. Offshore structures being

subjected to harsh environment, sensors are damaged often and leads to collapse of complete SHM unit. When a virtual sensing algorithm is used in conjunction with existing SHM unit, it improves the robustness of monitoring. Frequent retrofitting or replacing of sensors are not required as virtual sensing algorithm can estimate the response from unmeasured locations.

In addition to sensor malfunction, huge and complex offshore structure leads to large sensor network and inaccessible critical locations. Virtual sensing technique helps to reduce the number of sensors used, which eventually reduce the size of sensor network. Also, responses at critical locations shall be estimated using available measured responses. Thus using virtual sensing is inevitable to improve the robustness and reliability of SHM system.

2.3 Kalman filter

2.3.1 Random variables

Unlike the common mathematical variable, random variables are values subjected to variations due to chance. In other words random variable are simply a numerical representation of a random process / outcome. Random variables are broadly classified into two types: Discrete and continuous.

If a random variable can take only a finite number of possible values, then it is categorized as discrete. Best examples of discrete random variables are tossing a coin, rolling a die etc. In the case of continuous random variable it takes infinite number of possible values. Usually, measurements fall into this category. This section will discuss continuous random variables in detail. Random variables X are bounded by limit, where a and b are some constants. The chance of a random outcome is given by a probability density function. Following section will discuss normal or $G P(a < x < b)$ gaussian distribution in detail, other type of distributions are beyond the scope of this dissertation.

Figure 2.1. Shows probability density function of a normal distribution, a normal distribution is a very important statistical data distribution pattern occurring in many natural phenomena, such as height, blood pressure, lengths of objects produced by machines, etc. Certain data, when graphed as a histogram (data on the horizontal axis, amount of data on the vertical axis), creates a bell-shaped curve known as a normal curve, or normal distribution.

Normal distributions are symmetrical with a single central peak at the mean (average) of the data. The shape of the curve is described as bell-shaped with the graph falling off evenly on either side of the mean. Fifty percent of the distribution lies to the left of the mean and fifty percent lies to the right of the mean.

The spread of a normal distribution is controlled by the standard deviation. The smaller the standard deviation the more concentrated the data. The mean and the median are the same in a normal distribution.

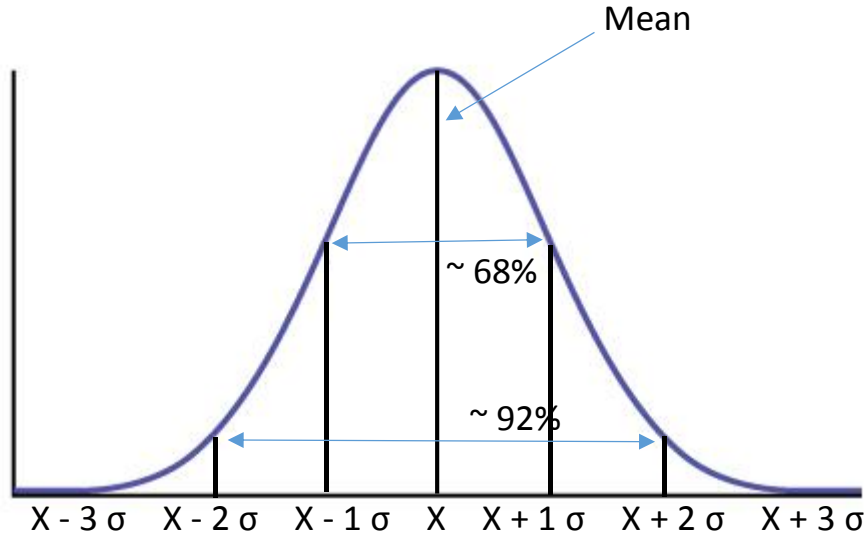


Figure 2.1. Normal distribution.

2.3.2 Kalman filter (state estimator)

Kalman filter was developed by Kalman (1960) [14], which is a set of mathematical equations that provides an efficient computational (recursive) means to estimate the state of a process, in a way that minimizes the mean of the squared error. It also estimates the unknown states based on the covariance relationship of states among each other. This paper aims in using the state estimation property of Kalman filter to predict unmeasured response in structures. Following sections will illustrate the mathematical formulation for general Kalman filter based state estimator.

Equation of motion of a linear dynamic system is given as:

$$\mathbf{M}\ddot{u}(t) + \bar{\mathbf{C}}\dot{u}(t) + \mathbf{K}u(t) = p(t)u(t) \quad (1.1)$$

where $u(t)$ is the displacement; its time derivatives $\dot{u}(t)$ and $\ddot{u}(t)$ are velocity and acceleration vectors, respectively; \mathbf{M} , $\bar{\mathbf{C}}$, and \mathbf{K} are the mass, damping and stiffness matrices of the dynamic system, respectively; and $p(t)$ is the input force vector.

Let $x(t)$ be the state vector given as

$$x(t) = \begin{Bmatrix} u(t) \\ \dot{u}(t) \end{Bmatrix} \quad (1.2)$$

Then, equation of motion is expressed in the state-space form as

$$\dot{x}(t) = \mathbf{A}x(t) + \mathbf{B}p(t) + \mathbf{G}w(t) \quad (1.3)$$

$$y(t) = \mathbf{C}x(t) + \mathbf{D}p(t) + \mathbf{H}w(t) + v(t) \quad (1.4)$$

where the matrices \mathbf{C} and \mathbf{D} in Eq. (4) are selected depending on the output of interest $y(t)$; Process and measurement noises $w(t)$ and $v(t)$ are assumed to be stationary, mutually uncorrelated stochastic process following the normal probability distribution $w \sim N(0, \mathbf{Q})$ and $v \sim N(0, \mathbf{R})$, respectively; the matrices \mathbf{G} and \mathbf{H} are the coefficients of process noise. The system matrices \mathbf{A} and \mathbf{B} are defined as:

$$\mathbf{A} = \begin{bmatrix} \mathbf{0} & \mathbf{I} \\ -\mathbf{M}^{-1}\mathbf{K} & -\mathbf{M}^{-1}\bar{\mathbf{C}} \end{bmatrix} \quad (1.5)$$

$$\mathbf{B} = \begin{bmatrix} \mathbf{0} \\ \mathbf{M}^{-1} \end{bmatrix} \quad (1.6)$$

For example, if all the displacement and acceleration are to be estimated, the matrices \mathbf{C} and \mathbf{D} can be defined as:

$$\mathbf{C} = \begin{bmatrix} \mathbf{I} & \mathbf{0} \\ -\mathbf{M}^{-1}\mathbf{K} & -\mathbf{M}^{-1}\bar{\mathbf{C}} \end{bmatrix} \quad (1.7)$$

$$\mathbf{D} = \begin{bmatrix} \mathbf{0} \\ \mathbf{M}^{-1} \end{bmatrix} \quad (1.8)$$

A Kalman filter-based state estimator can be built to estimate the state $x(t)$

$$\dot{\hat{x}} = \mathbf{A}\hat{x} + \mathbf{B}p + \mathbf{L}(z - \mathbf{C}\hat{x} - \mathbf{D}p) \quad (1.9)$$

where \hat{x} is the estimated state of the state estimator, \mathbf{L} is the Kalman gain, and z is the limited physical measurement. The Kalman gain \mathbf{L} is defined as:

$$\mathbf{L} = \left[\mathbf{P}^* \mathbf{C}^T + \mathbf{G} \mathbf{Q} \mathbf{H}^T \right] \left[\mathbf{R} + \mathbf{H} \mathbf{Q} \mathbf{H}^T \right]^{-1} \quad (1.10)$$

where the error covariance P^* is obtained by minimizing the steady state error covariance.

$$P^* = \lim_{t \rightarrow \infty} E\left(\{x - \hat{x}\}\{x - \hat{x}\}^T\right) \quad (1.11)$$

In summary, the above discussions provides information about Kalman filter in sate estimation. Note, in addition to state estimation, Kalman filter is also a better platform for data fusion. Data fusion basically means combining various sensor measurements. Usually sensors with contrasting performances are combined to compensate each other's weakness. Generally piezo type of sensor (accelerometers) perform well in high frequency region. Where else sensors like Laser Displacement Sensor (LDS), strain gauges, ext. are good only in low frequency region. By combining these sensors measurements under a suitable platform (Kalman filter) can provide an overall better performance [17], and [18]. Park et al (2013), [19] used this technique to estimate displacement by combining strain and accelerometer further this technique is reported by many researchers to improve estimation accuracy.

Chapter 3

DATA FUSION APPROACH FOR NON-STATIONARY RANDOM INPUTS

Random input is common among mechanical and civil structures. These structures are subjected to environmental loadings such as wind, traffic, human load, earthquake, tidal current, etc. Unlike the other loadings, tidal and wind loading are mostly non-stationary random inputs. Offshore structures being subjected to non-stationary random inputs, it is important to analyze the behavior of structure under non-stationary random input. Figure 3.1 shows the sample stationary and non-stationary random input. As the figure illustrates, for a stationary random input, the input history is distributed about zero (i.e. Mean of input history). In the case of non-stationary random input, mean of the input history is non-zero. This shows structures subjected to non-stationary input have higher chance of failure.

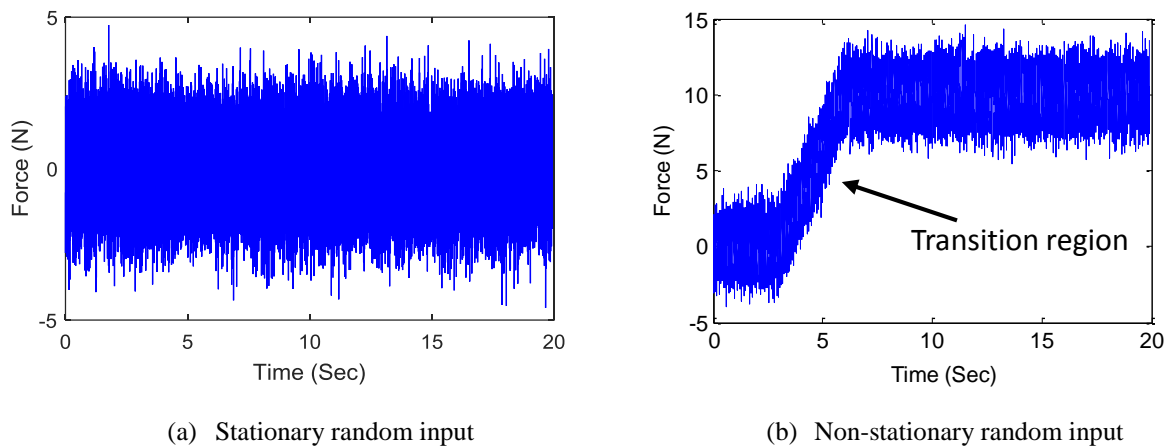


Figure 3.1 Types of random input

Monitoring the offshore structures under water is unique in that the sensor installation and maintenance associated with the data acquisition are quite challenging because critical structural members are often inaccessible. Furthermore, the repeated strong tidal current can easily cause sensor malfunctioning. Estimating structural responses at unmeasured important locations can be a powerful alternative to the direct measurement when it becomes unavailable. Despite the usefulness of the response estimation, it has not been fully explored in the literature yet. As this dissertation focuses on monitoring the offshore structures, we consider two major aspects that need to be appropriately addressed:

- 1) Offshore structures are continuously subjected to non-stationary random input excitations

- 2) Sensors are prone to get damaged due to the harsh environment or difficult to install in some hot spots

The input forces as well as the structural responses have a slowly varying, large amplitude trend according to the changing direction of the tidal current. Thus, the response estimation algorithm should be capable of handling non-stationary random inputs and estimate response with limited measurements [20].

The Kalman filter-based state estimator to capture structural responses due to the non-stationary random input is outlined here. The Kalman filter provides an efficient computational means to estimate the state of a process in a way that minimizes the mean of the squared error. This paper uses the state estimation property of Kalman filter to predict unmeasured response in a structure. Equation of motion of a linear dynamic system is given as: Q

$$\mathbf{M}\ddot{u}(t) + \mathbf{\bar{C}}\dot{u}(t) + \mathbf{K}u(t) = p(t) \quad p(t) \tag{3.1}$$

where $u(t)$ is the displacement; it's time derivatives $\dot{u}(t)$ and $\ddot{u}(t)$ are velocity and acceleration vectors, respectively; \mathbf{M} , $\mathbf{\bar{C}}$, and \mathbf{K} are the mass, damping and stiffness matrices of the dynamic system, respectively; and $p(t)$ is the input force vector.

Because the input information in offshore structures are practically impossible to measure, the algorithm is designed to work without input information. It is assumed that there is no input given to the system ($p(t)=0$) rather the input is assumed to be only from the process noise $w(t)$. Furthermore, process noise covariance is modified as the covariance of input to incorporate the effect of non-zero mean input. (see Figure 3.2)

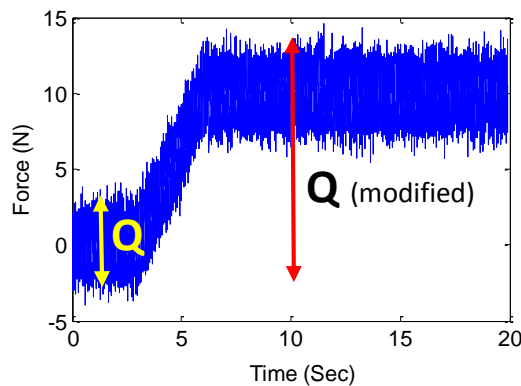


Figure 3.2. Non-stationary random input with modified covariance

Following Eqs. (3.2) and (3.3) give the state space model of the system.

$$\dot{x}(t) = Ax(t) + Bw(t) \quad (3.2)$$

$$y(t) = Cx(t) + Dw(t) + v(t) \quad (3.3)$$

where the matrices C and D in Eq. (3.3) are selected depending on the output of interest $y(t)$; Process and measurement noises $w(t)$ and $v(t)$ are assumed to be stationary, mutually uncorrelated stochastic process following the normal probability distribution $w \approx N(0, \mathbf{Q})$ and $v \approx N(0, \mathbf{R})$, respectively; the matrices A and B are system matrices. With the above state space model Kalman state estimator is constructed as

$$\dot{\hat{x}}(t) = A\hat{x}(t) + L(z - C\hat{x}(t)) \quad (3.4)$$

$$y(t) = C\hat{x}(t) \quad (3.5)$$

where z is the measured responses and Kalman gain L can be expressed as

$$L = [P^*C^T + BQD^T][R + DQD^T]^{-1} \quad (3.6)$$

where the error covariance P^* is obtained by minimizing the steady state error covariance.

$$P^* = \lim_{t \rightarrow \infty} E\left(\{x - \hat{x}\}\{x - \hat{x}\}^T\right) \quad (3.7)$$

P^* is obtained by solving the algebraic Riccati equation which uses the modified noise covariance Q . Note that for a given non-zero mean input, the response/output is expected to be non-zero mean which may include multiple steady state and transition stages in time domain. In order to estimate such a complex response, the error covariance P^* in Eq. (3.7) should minimize the steady state error covariance at all the stages in the response. The modified process noise Q enables P^* to minimize steady state error covariance at all the stages in the response; this enables the formulation to handle non-zero mean input and responses properly.

From Eq. (3.4), it can be inferred that value of filter gain L determines the priority between model and measurements in response estimation. From Eq. (3.6) for a given model (A , B , C , and D) and process noise Q , the filter gain L is inversely proportional to the measurement noise covariance R . Thus, estimation

using sensors with lower noise level will depend more on measured responses than the given model and vice versa for sensors with higher noise floor. Thus, using sensors with lower noise floor gives better estimation in situations where available numerical model is not accurate.

Thus, modifying Q shall enable the algorithm to capture large deviations in states, but the major source that enables virtual sensing to handle non-stationary response is data fusion. Unlike the stationary random response, non-stationary responses have frequency content dominated near zero and at other resonate frequencies (see Figure 3.3), thus measured signals should be able to cover all the frequency content. Figure 3.3 shows the frequency content of stationary and non-stationary random signal shown in Figure 3.1. From the figure it is clear that non-stationary random signals have frequency content dominated near zero and at other resonate frequencies. Hence the fundamental idea of this dissertation is to combine sensors that perform well in low and high frequency region to accomplish the task of handling non-stationary random responses.

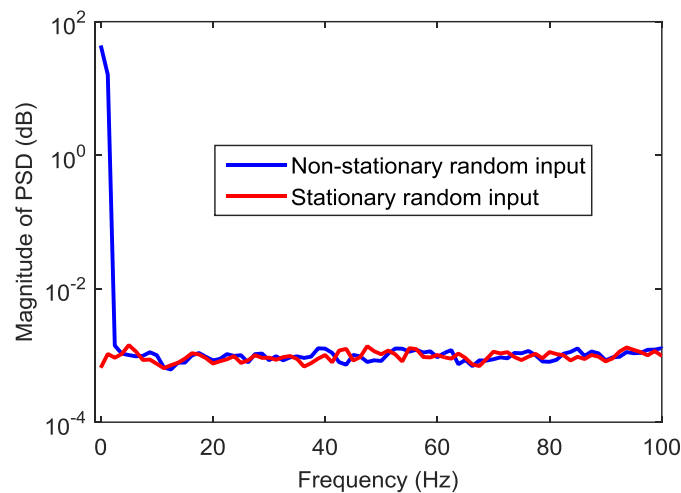


Figure 3.4 Frequency domain comparison of stationary and non-stationary random signal

In the following validations, input information is assumed as unmeasured and input covariance is estimated from measured responses. In addition, four types of measurement combinations are used for the response estimation at the unmeasured locations: strain only, acceleration only, acceleration and strain, and acceleration and tilt. The combination of acceleration with strain or tilt (i.e., angular displacement) is considered for the data fusion, because acceleration captures the high frequency behavior of the structure in accuracy, while the strain and tilt can compensate the weakness in low frequency behavior and eventually increase the accuracy of estimation. For the four types of response combinations, the best combination is obtained by assessing the accuracies of the estimated responses.

Chapter 4

NUMERICAL AND EXPERIMENTAL VALIDATION

This chapter validates the Kalman filter-based virtual sensing method with a simply supported beam and a bottom fixed offshore model. Virtual sensing is validated both numerically and experimentally. Response under non-stationary random input is collected from limited locations and used in virtual sensing algorithm to estimate responses at unmeasured locations.

4.1 Validation with simply supported beam

4.1.1 Numerical validation

In this section, a numerical model of a simply supported beam is considered to estimate strain responses from limited measurements using the modified Kalman state estimator.

4.1.1.1 Simulation setup

A simply-supported Finite Element beam model was developed using MATLAB. The beam is composed of 20 Euler-Bernoulli beam elements each of which has the length of 0.1 m as shown in Figure. 4.1. The element has a rectangular cross-section of 1cm thickness and 10 cm width. The Young's modulus and density of the material were selected as 206 GPa and 7580 kg/m³ respectively. To analyze the effect of model error on the virtual sensing accuracy, another numerical model is prepared with slight perturbation from the actual model. Perturbation in the new model is introduced by changing the elastic modulus and moment of inertia. Figure. 4.2 shows the comparison of frequency response functions (FRFs) from the simulation model and a model used in the virtual sensing algorithm, where natural frequencies of both the model are different.

The originally developed numerical model was used in MATLAB Simulink to simulate the acceleration, strain and angular displacement responses of the beam under a non-stationary random input shown in Figure 4.3 is applied at node 18. These responses sampled at 853 Hz with elliptic AA filter were used as reference response. The accelerations, strains, and tilt from a few selected nodes were contaminated by white noise. Accelerations and tilt are contaminated by 2% noise in root mean square (RMS), while the strains are contaminated by 10% noise in RMS based on the experience of higher noise on the actual strain measurement.

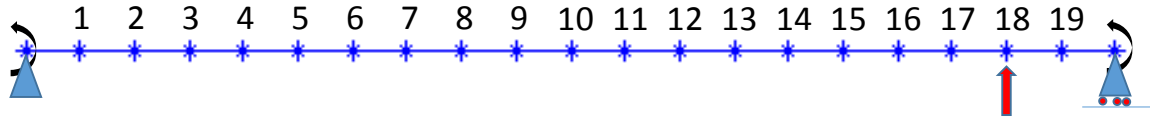


Figure. 4.1 Simply supported beam model

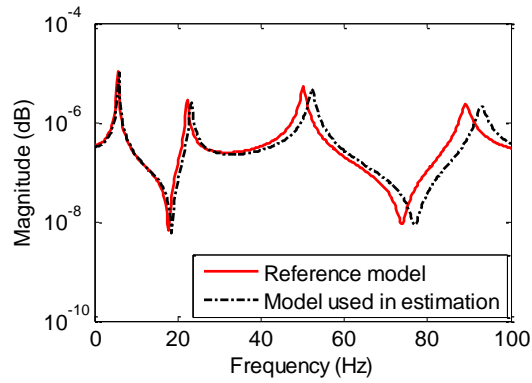


Figure. 4.2 Comparison of FRFs between the reference and the perturbed models

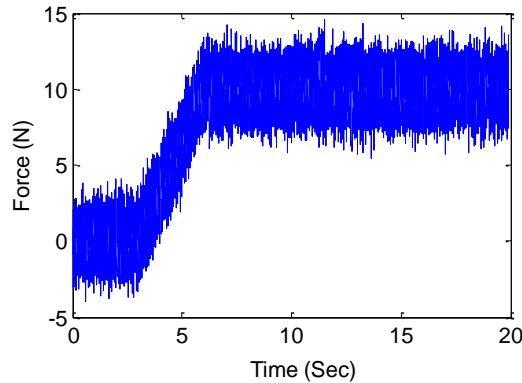


Figure. 4.3 Non-zero mean input excitation

4.1.1.2 Simulation cases

To verify the virtual sensing performance, four types of measurements are considered as shown in Figure. 4.4. Cases 1 and 2 use strains and accelerations at nodes 5, 10, 15, and 18, respectively. Case 3 uses both accelerations and strains at nodes 15 and 18, and Case 4 uses two accelerations at nodes 15 and 18 and one tilt response at node 10. Node 12 is the unmeasured location whose strain is to be estimated.

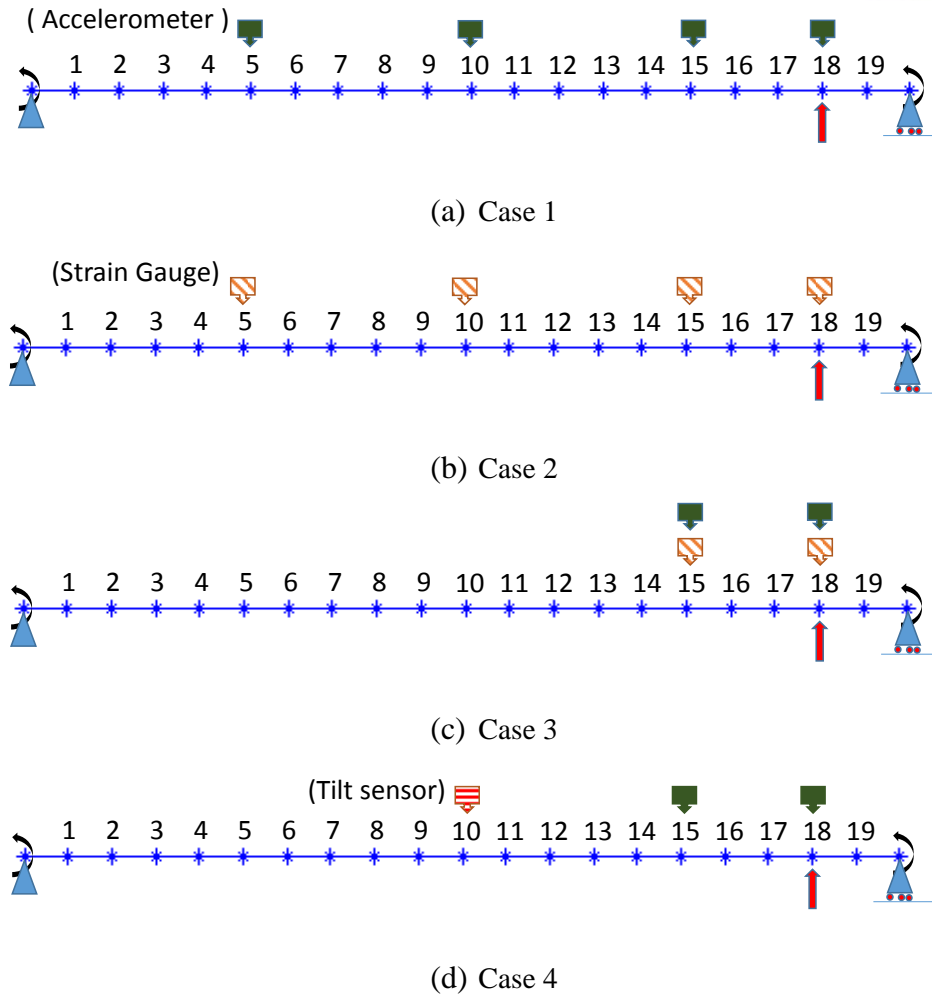


Fig. 4.4 Four measurement cases

4.1.1.3 Results

Figures. 4.5 and 6 show the estimated strain at node 12 in the time and frequency domains, respectively. Figure. 4.5 shows the estimated strain responses that have non-stationary response in more or less accurate, except the Case 2 produces the zero-mean one whose quasi-static trend is unidentified. The result is consistent with the fact that given acceleration in the simulation does not contain the quasi-static behavior of the measured structure. Figure. 4.5 also shows that the multi-sensor cases (i.e., Cases 3 and 4) can better estimate the strain than the sole use of responses (i.e., Cases 1 and 2). Further comparing the multi-sensor data cases to each other, the combination of acceleration and tilt resulted in more accurate estimation than the combination of acceleration with strain. Eq. (2.9) infers that the Kalman gain gives priority to measurement (i.e., tilt) combined with acceleration than response predicted from the model, when the

measurements are less contaminated. Thus, Case 4 whose measurement has lower noise is less affected by the model error in the estimation than the other cases, as shown in Figure. 4.5.

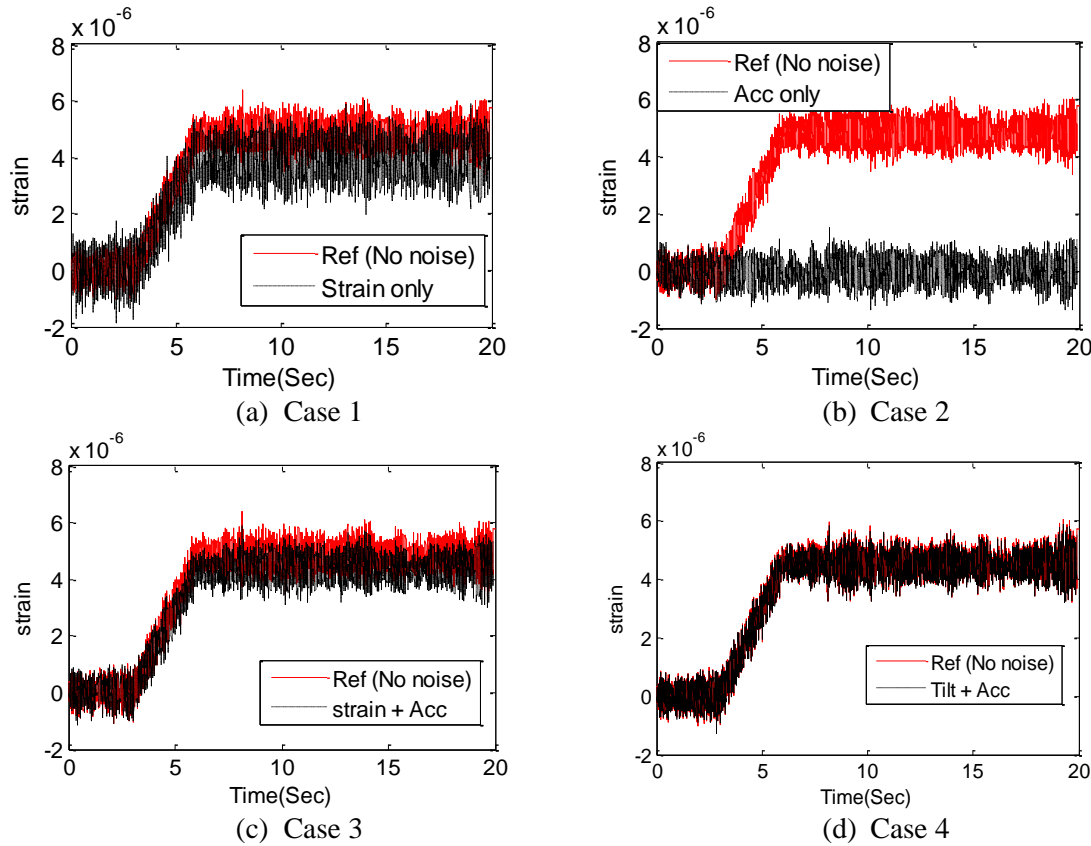


Figure. 4.5 Estimated and reference strain responses in time domain at node 12

The accuracy that is visually assessed in time domain as shown in Figure. 4.5 is investigated in frequency domain (see Figure. 6). For all measurement cases, four peak frequencies under 100 Hz (i.e., 5.8, 23.3, 52.1, and 92.9 Hz) are exactly estimated despite the model used for the Kalman state estimator is inexact. This shows that the virtual sensing method has the robustness to the model error that is compensated due to using the measurements. The discrepancy is, however, observed in the anti-resonant frequency regions. In Figure. 4.6(b), Case 2 that uses only acceleration data has poor agreement with exact strain in the low frequency region under the first peak frequency, which reveals the failure in capturing the quasi-static trend in the strain. Whereas Case 1 (see Figure. 4.6(a)) has comparatively good agreement near 0 Hz, it has a higher noise floor compared to the reference. Comparing to Cases 3 and 4 (see Figures. 4.6(c) and (d)), Case 4 that uses two accelerations with one tilt shows better agreement in both high and low frequency regions than Case 3 that uses two accelerations with two strains.

To investigate the consistency of the virtual sensing method based on the Kalman filter, the strain responses were estimated for all locations. Instead of showing all the estimated responses compared with the exact ones, root mean square errors (RMSEs) between reference and estimated strains were calculated as:

$$Error = \frac{\sqrt{\sum(\varepsilon_{est} - \varepsilon_{ref})^2}}{\sqrt{\sum(\varepsilon_{ref})^2}} \quad (4.1)$$

where ε_{ref} is the reference strain and ε_{est} is the estimated strain.

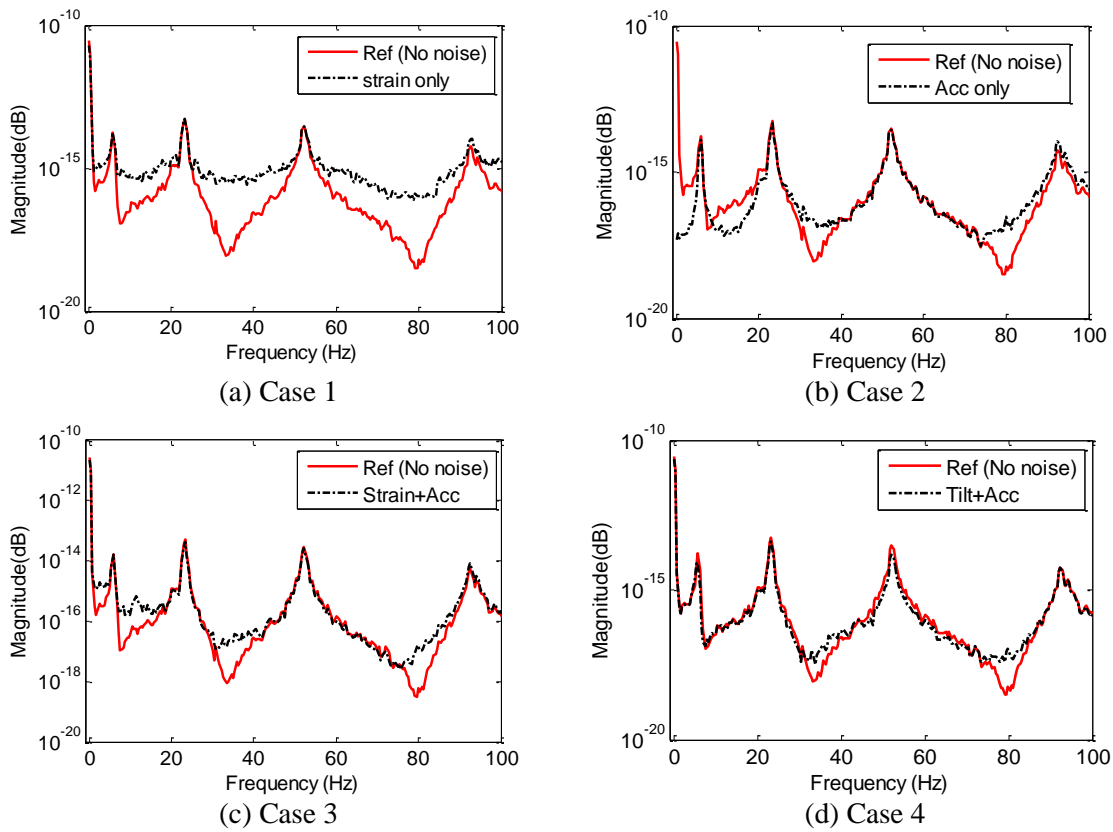


Figure. 4.6 Estimated and reference strain responses in frequency domain at node 12

Figure. 4.7 shows the RMSEs calculated for all nodes. Note that the RMSEs of Case 2 were quite large compared to the others due to inaccurate estimation of quasi-static strain component, and thus they were not plotted together. As to Case 1, the RMSEs are not consistent for all nodes and higher than those from Case 3 and Case 4, because during Kalman estimation of Case 1 a higher priority is given to erroneous model then the measurements due to higher noise floor. Case 4 has lower error for all nodes because the tilt contains lower level of noise than the strain used in Cases 1 and 3.

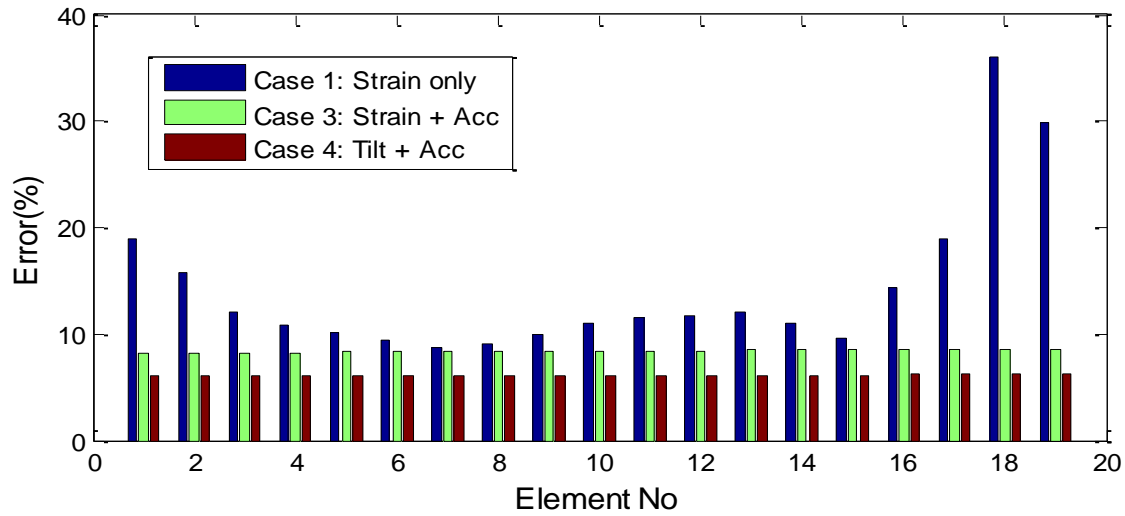


Figure. 4.7 Error of estimated strains at all nodes

4.1.2 Experimental validation

The section describes the laboratory-scale experiment for response estimation that is designed to replicate the numerical simulation.

4.1.2.1 Simulation setup

Figure. 4.8 shows the test beam whose length, width, and thickness are 2m, 10cm, and 1cm, respectively. The Young's modulus and density of the beam are 206 GPa and 7860 kg/m³, respectively. Since the test beam resembles the numerical beam in Figure. 4.1, the node number is assigned for every 0.1 m as Figure. 4.1. The test beam was excited with a non-zero mean force similar to Figure. 4.3 made by a shaker installed at node 18 (i.e., 0.2 m apart from the right support).

Four different experimental cases are performed and sensor deployment in each case is similar as in section 4.1. All the responses were sampled at 5 KHz using National Instruments data acquisition system (DAQ). Input voltage generated from DAQ was amplified using an amplifier and supplied to the shaker, and the responses from strain gauges, accelerometers and a tilt sensor were obtained simultaneously using the DAQ. Figure 4.9 shows the difference between the FRFs from the experiment and the numerical model. The disagreement of the FRFs clearly shows the eligibility of inaccurate numerical model used in response estimation.

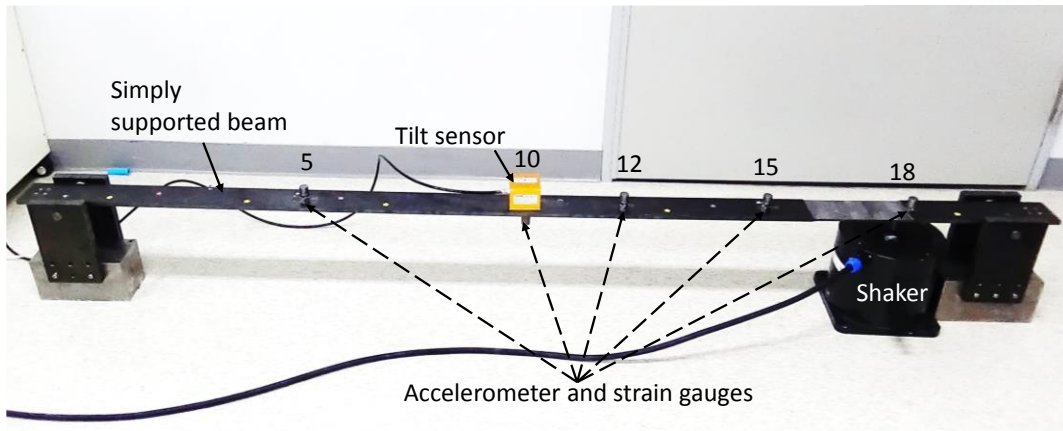


Figure. 4.8 Experimental beam structure with sensor and actuator

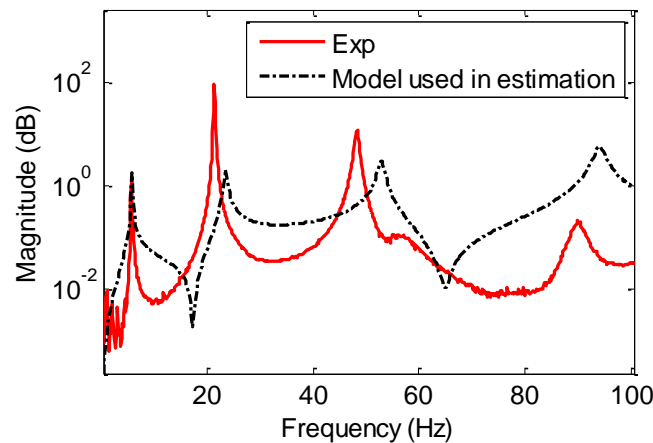


Figure. 4.9 Comparison of FRFs from experiment and numerical model

4.1.2.3 Results

Figure. 4.10 shows the estimated strain responses according to four measurement cases compared to the measured strain at unmeasured node 12. Similar to the numerical simulation, all Cases estimated the strain response at the unmeasured node with somewhat accuracy, except Case 2.

Case 2 (see Figure. 4.10(b)) shows the inability of acceleration data to estimate the gradually increasing strain response. Case 1 (see Figure. 4.10(a)) resulted in the estimated strain with high noise level, while the multi-metric cases (i.e., Case 3 and Case 4) have lower noise levels (see Figures. 4.10(c) and 4.10(d)). Among the multi-metric Cases, Case 3 could not estimate exact quasi-static response, while Case 4 resulted in the estimated strain with better agreement to the measured strain due to lower noise level of the tilt sensor than the strain gauges in practice.

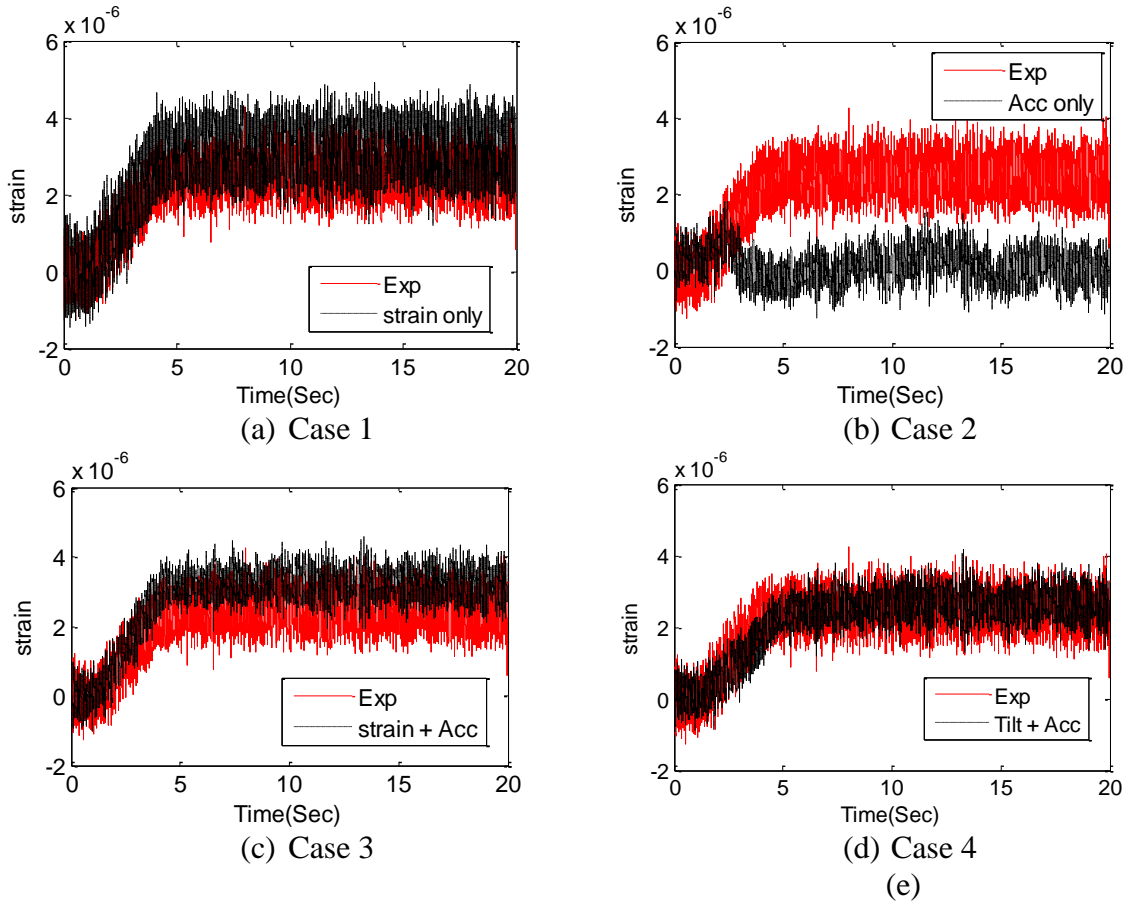


Figure. 4.10 Estimated and measured strain responses in time domain at node 12

Figure. 4.11 is the comparison of estimated responses in the frequency domain. Note that the peak at 60Hz in the measured strain is from the electrical noise around the laboratory where the experiment was carried out. First, unlike the reference strain used in the numerical simulation, the measured strain to be used as a reference contains high level of noise represented by flatness at the anti-resonant regions. This is the evidence why the strain was contaminated by higher level of noises than the other responses in the numerical simulation. Figure. 4.11(b) clearly shows that Case 2 has poor agreement in the low frequency region (near 0 Hz) related to quasi-static component of strain compared to other methods. Figures. 4.11(a,c,d) show reasonable agreement of resonant peaks at 6.4, 22.6, 50.0, and 88.8 Hz, while there are some differences in the anti-resonant frequency regions. Among the results, Case 4 (see Figure. 4.11(d)) has the lowest level of noises at anti-resonant regions.

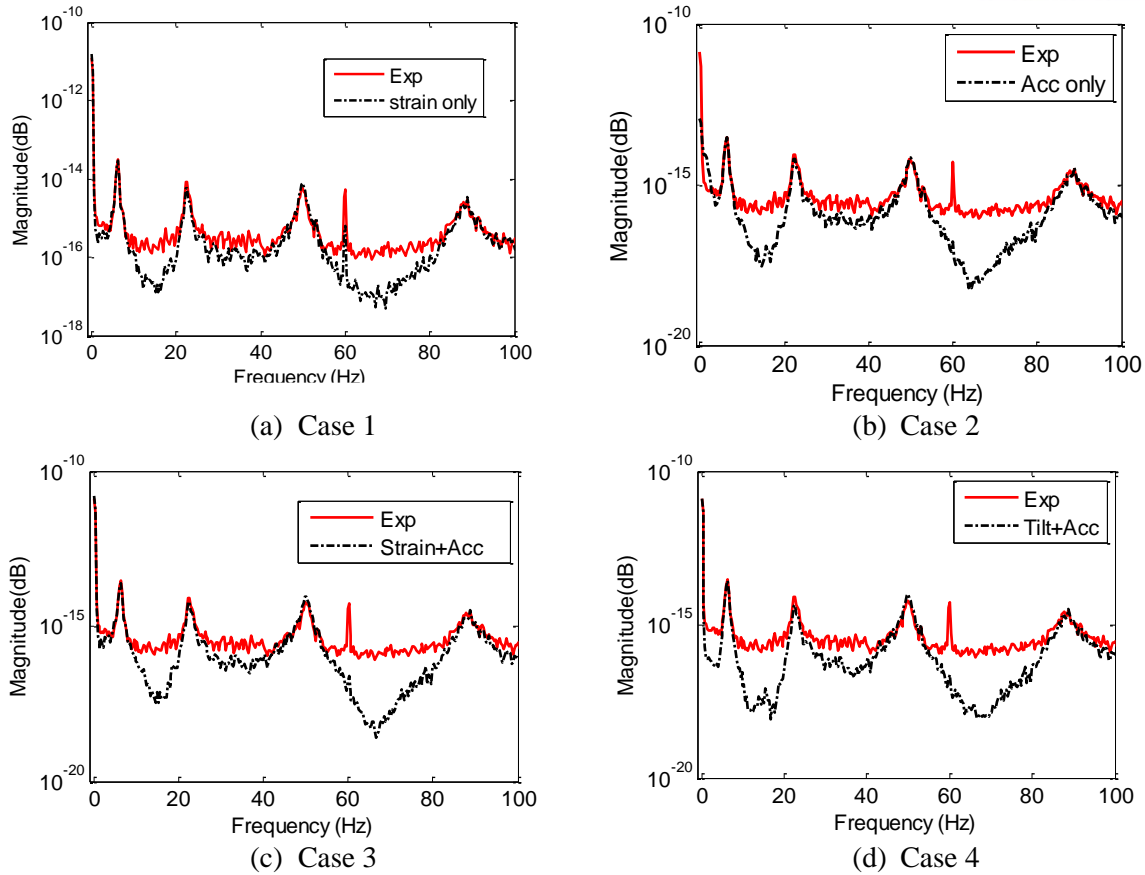


Figure. 4.11 Estimated and measured strain responses in frequency domain at node 12

Figure. 4.12 shows the RMSEs between estimated and selected measurement strains. Note that the RMSEs of Case 2 are much larger than the others due to inaccurate quasi-static strain components, and thus they are not plotted together. Similar to Figure. 7, RMSEs from the numerical simulation, Case 4 showed smallest RMSEs less than 5%. Cases 1 and 3 are influenced by model error and noisy strain measurement, and thus higher RMSEs are estimated. Note that the RMSEs of Case 3 is slightly larger than those of Case 1 at several elements unlike the RMSEs of the numerical simulation shown in Figure. 4.7, because the reference strain used for comparison contains measurement noise in the experiment.

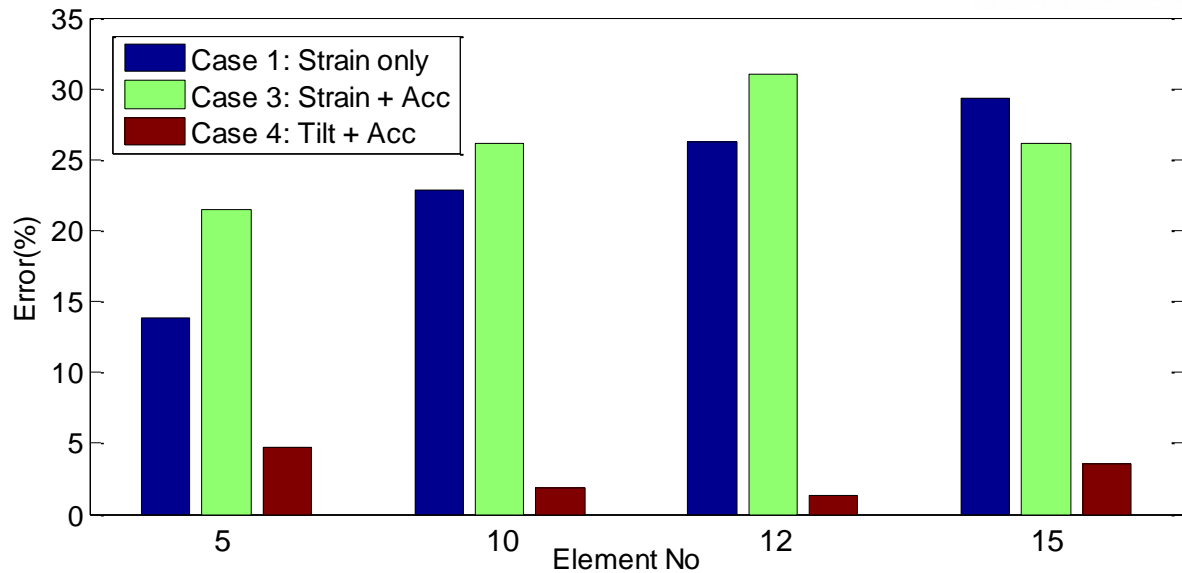


Figure.4.12 Error in estimated strain

4.2 Validation with model of bottom fixed offshore structure

This section validates the virtual sensing technique with a model of bottom fixed offshore structure. Validation is performed both numerically and experimentally. Both validations are delineated in the following sub-sections.

4.2.1 Numerical validation

In this section, a numerical model of offshore structure (see Figure. 4.13) is developed. This model is simulated with MATLAB Simulink under realistic input situation. Limited responses were collected and used in Kalman filter based response estimation algorithm to estimate the unmeasured response.

4.2.1.1 Simulation setup

The model is composed of 24 frame elements each of which has the length of 0.2 m as shown in Figure. 4.13. the columns (C1, C2, C3, and C4) has a circular cross-section of radius 3 cm. The Young's modulus and density of the columns were selected as 1000 MPa and 953 kg/m³ respectively. Four frame members on top of the columns has Young's modulus and density of 210 GPa and 7850 kg/m³. The developed numerical model was used in MATLAB Simulink to simulate the acceleration and strain responses under a non-zero mean input. Inputs are applied to first two nodes of each columns as shown in Figure. 4.13. to simulate the real situation columns in upstream and downstream experience similar forces. Responses are

sampled at 150 Hz with elliptic AA filter. The accelerations and strains from a few selected nodes were contaminated by white noise. Accelerations are contaminated by 2% noise in root mean square (RMS), while the strains are contaminated by 10% noise in RMS based on the experience of higher noise on the actual strain measurement. These limited responses are used to predict the input covariance and also the unmeasured responses.

From chapter 3 it is clear that the input covariance information is important for response estimation. With the help of numerical model a transition matrix is constructed from strain to the input force. Using this relation, the measured strain responses can be transformed to the input forces.

$$P(t) = K_{SP} \mathcal{E}(t) \quad (4.2)$$

where K_{SP} is the transition matrix from strain to the input force. To estimate input covariance, strain at unmeasured location is assumed to be same as nearest available strain response. With this assumption input time history is calculated from Eq. 4.2. As discussed in chapter 4 sensors with lower noise level enables Kalman filter to give higher priority to measurements thus even with inaccurate input covariance, Kalman filter could make a better estimate. Strain gauges are sensitive to electrical noises and local defects in the structure. Acceleration being a poor low frequency observer, the quasi-static trend of non-stationary responses is generally difficult to capture in comparison to strain gauges. Thus Fusion of multi-metric data (strain and acceleration) will enhance the accuracy of response estimation [17], and [18].

Four simulation cases are considered here, in each case, one of the strain responses is estimated with the help of other strain and acceleration responses. For example in case 1, strain measurements near the root of column 2, 3 and 4 and acceleration on top (Ref. Figure. 4.13) are used to estimate the strain response in column 1.

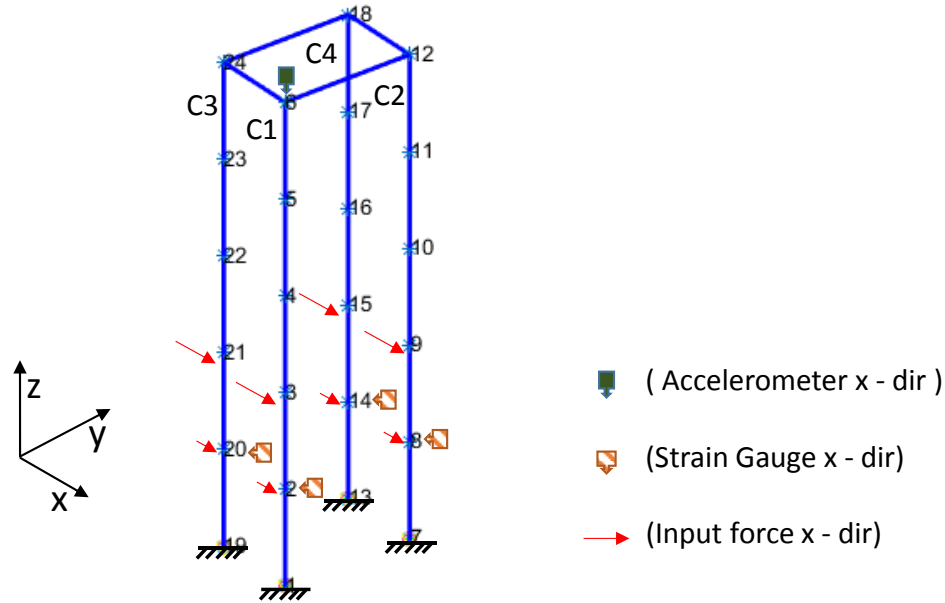


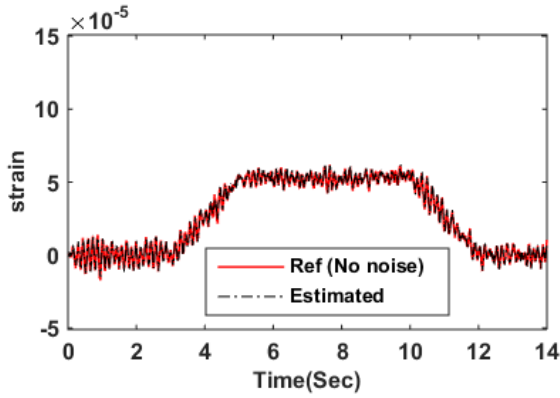
Figure. 4.13. Numerical model

4.2.1.2 Validation results

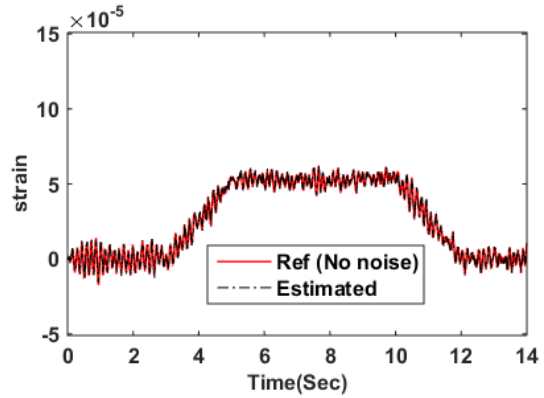
Figure. 4.14 shows the estimated strain in each case. Each case is processed in two steps. Step 1: estimate the input covariance. Step 2: use the estimated input covariance and limited measurements in Kalman filter based state estimator to estimate the unmeasured response. In case 1, strain responses from nodes 8, 14 and 20 with acceleration responses from node 6 are used to estimate the strain at node 2. During input covariance estimation step response at unmeasured node 2 is replaced by 8, as they experience a similar force. A similar procedure is followed to estimate strain response at other columns (Table. 4.1). From the Figure. 4.14 estimated non-zero mean strain at each column is in good agreement with the reference strain. Column 3 and 4 experience higher strain due to upstream force compared to column 1 and 2. Figure. 4.15 shows the capability of algorithm to estimate the dynamic component of response.

Table. 4.1. Measured and estimated response for each case.

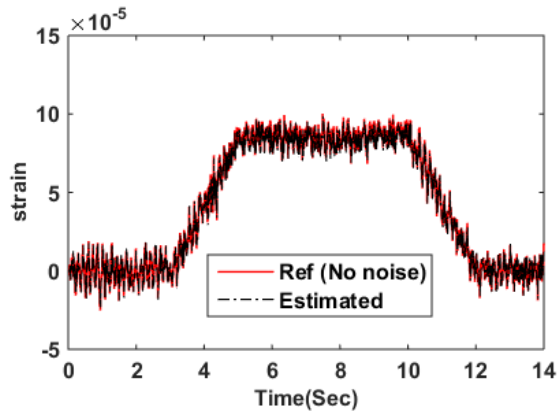
Case	Measured strain location	Measured acceleration location	Estimated strain location
1	8, 14, and 20	6	2
2	2, 14, and 20	6	8
3	2, 8, and 20	6	14
4	2, 8, and 14	6	20



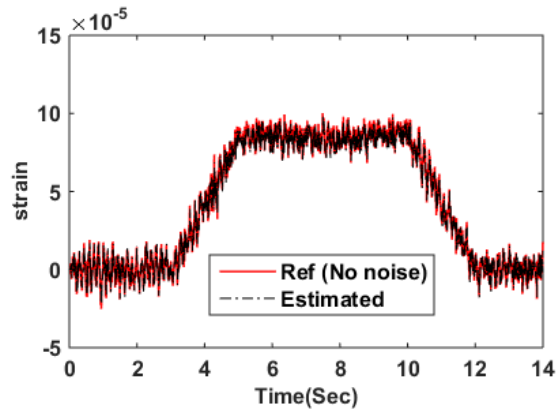
(a) Case 1



(b) Case 2



(c) Case 3



(d) Case 1

Figure. 4.14 Estimated and reference strain response in time domain

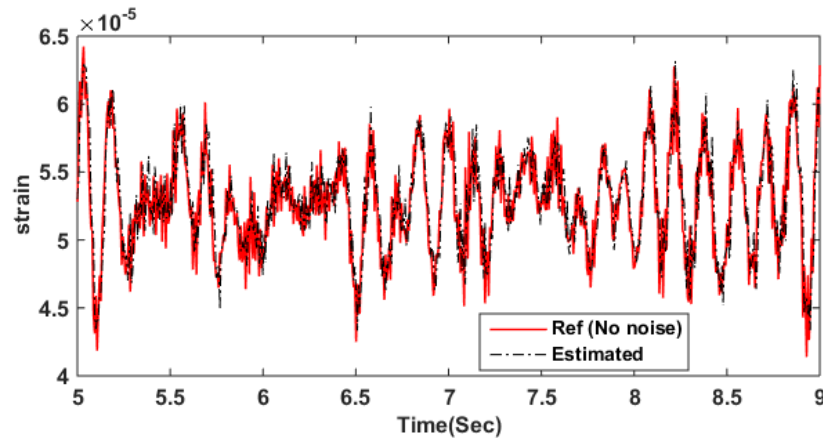


Figure. 4.15 Estimated and reference strain response in column 1 (between 5 and 9 sec)

In addition to the comparison in the time domain, the estimated and measured strain responses are compared in the frequency domain by plotting their power spectra as shown in Figure. 4.16. Note that only case 1 is shown as all cases exhibit similar power spectra. From the Figure. 4.16, it can be observed that the estimated strain is in a good agreement with the reference strain. Their strong agreement near 0 Hz shows the capability of algorithm to handle non-zero mean responses.

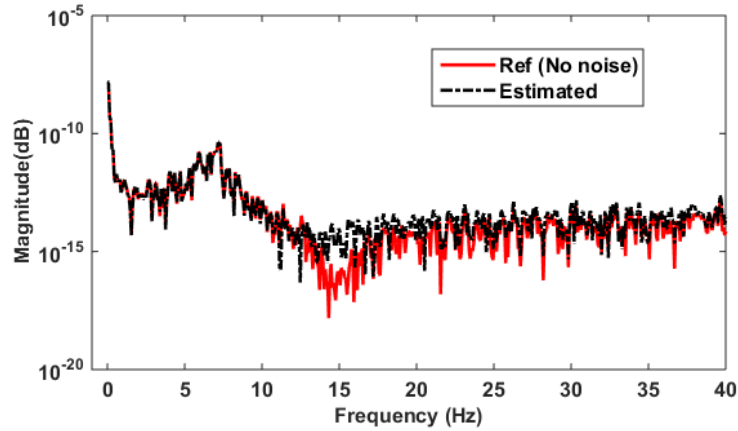


Figure. 4.16. Estimated and reference strain response in frequency domain.

To investigate the consistency of the response estimation, root mean square errors (RMSEs) between reference and estimated strains were calculated as:

$$Error = \frac{\sqrt{\sum (\varepsilon_{est} - \varepsilon_{ref})^2}}{\sqrt{\sum (\varepsilon_{ref})^2}} \quad (4.3)$$

where ε_{ref} is the reference strain and ε_{est} is the estimated strain. Figure. 4.17 shows the RMSEs calculated at each column. Error in estimation for each column is less than 1 %.

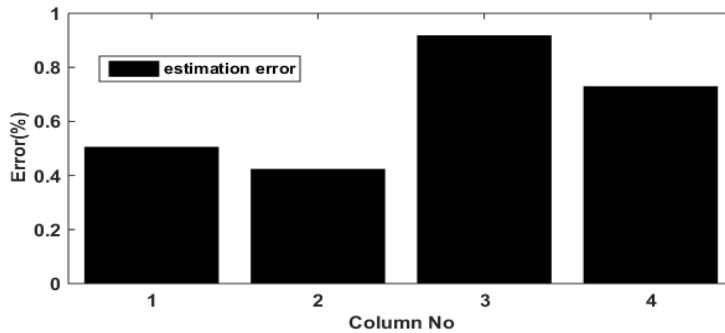


Fig. 4.17. Error of estimated strain in each column.

4.2.2 Experimental validation

This section experimentally validates the algorithm with a model of offshore structure. The experiment is conducted in a flume with controlled water current. Measured responses are used to validate the response estimation algorithm.

4.2.2.1 Experimental setup

Experiment was carried out in a circulating water channel as shown in Figure. 4.18. Length, width, and height of the circulating water channel are 24 m, 480 mm, and 900 mm respectively. Specimen was installed 9 meters away from the sluice gate to avoid the effect of reflected water current from sluice gate and also to ensure a uniform flow from source.

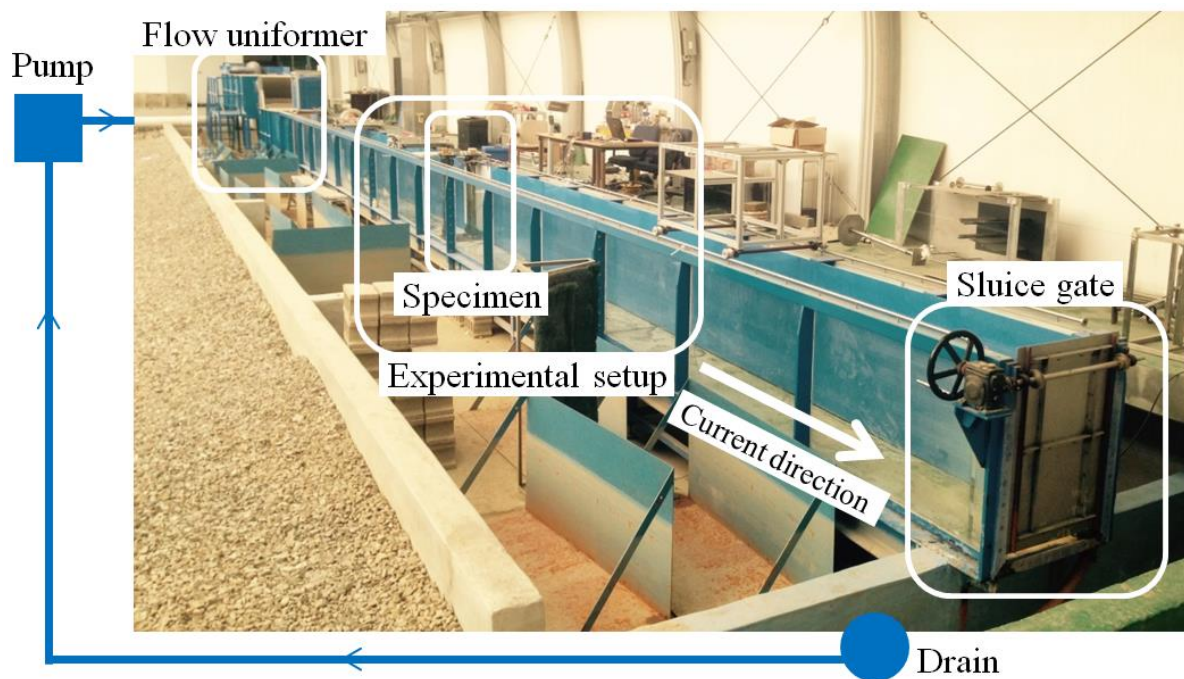


Fig.

Figure 4.18. Circulating water channel setup

Figure. 4.19 shows the dimension of specimen and the sensors deployed on it. The selected accelerometers are integrated circuit piezoelectric (ICP) Type 355B33, PCB Piezotronics, Inc. Strain gauges were deployed on each column at 150 mm from the root of the specimen. As the velocity of water current is lower at the root of column, Strain gauges are installed near the root to avoid getting damaged. Also, waterproof material was applied to avoid distortion of the strain response. Strain gauges are configured with half-bridge to improve its sensitivity. The acceleration and strain responses were measured with a sampling rate of 200

Hz by data acquisition devices (DAQ), produced by HBM, Inc., QuantumX 1601b and 1615b (Operation manual).

The side view of the specimen

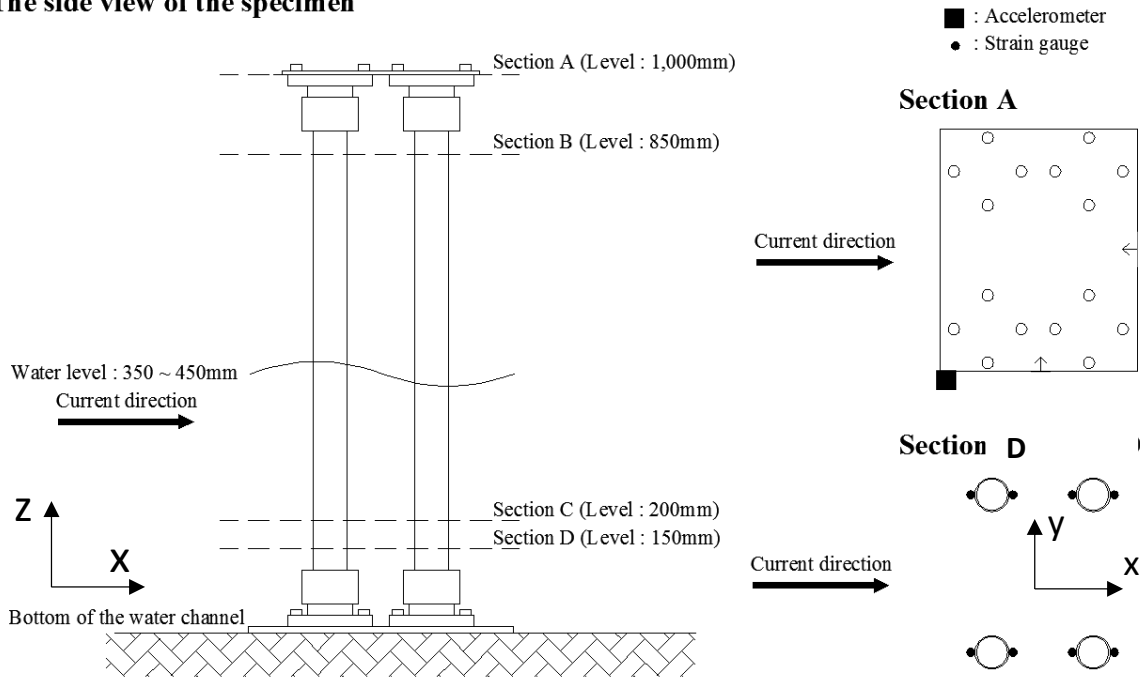


Fig. 4.19. Specimen with deployed strain gauge and accelerometer

Figure 4.20. Shows the specimen with and without water current. It can be observed that the upstream water level is higher than the downstream. Also the columns in the downstream experience some turbulence compared to other columns. Thus columns in upstream and downstream will experience different force.

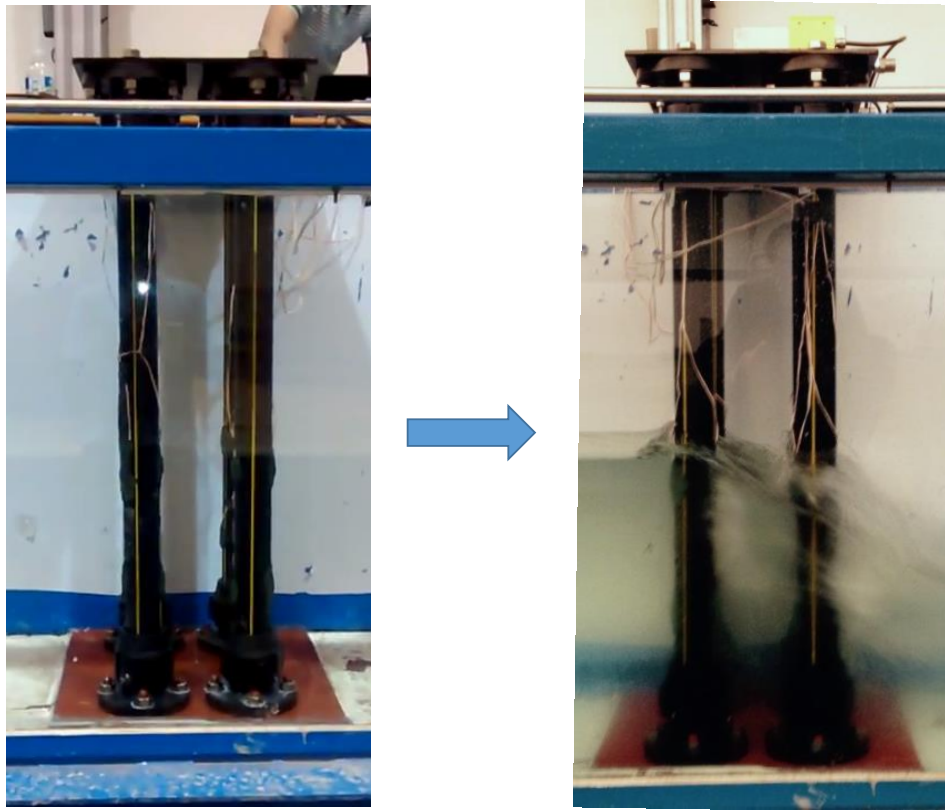


Figure. 4.20. Specimen with and without water current

Table 4.2 shows material properties and the dimension for the top plate and columns which are parts of the experimental specimen.

TABLE 4.2. Material properties and the dimension for the experimental specimen

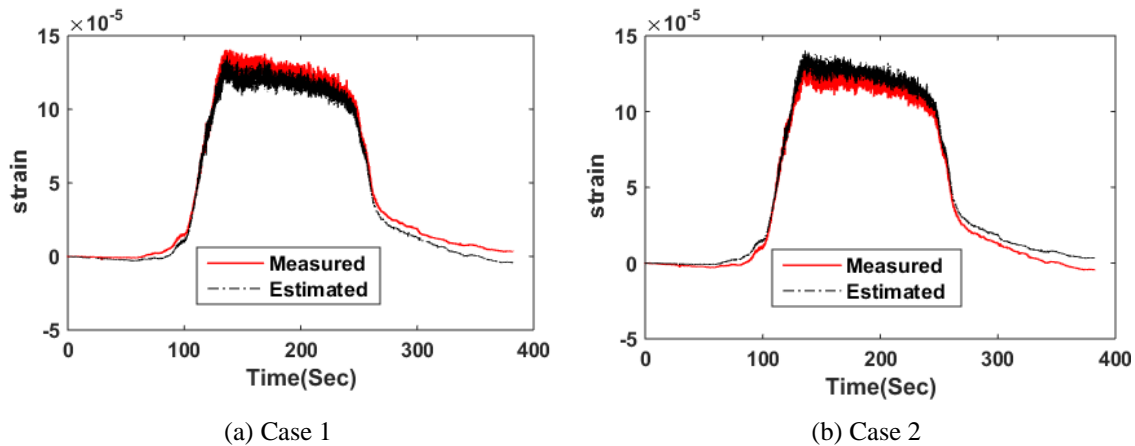
Properties	Top plate	Columns
Material	Steel	HDPE (high-density polyethylene)
Young's modulus	210 GPa	1000 MPa
Shear modulus	79.3 GPa	800 MPa
Density	7850 Kg/m ³	953 Kg/m ³
Size	430mm x 350mm x 9t	D60mm x 5t height : 1000mm
Weight	10.63kg (without accessories)	0.823kg/each column (without connector)

The experiment is carried out in 3 steps: Step 1: Initially the flume is filled with a water level of 400mm by shutting the sluice gate at the end of the water channel (see Figure. 4.18). Step 2: Now the pump is turned

on and also the sluice gate is controlled to maintain the same water level throughout the experiment. Step 3: after few minutes pump is turned off and simultaneously sluice gate is controlled to maintain the same water level.

4.2.2.2 Estimation results

Figure. 4.21 compares the experimental and estimated strain response at each column. Validation cases here are similar to the cases seen in numerical validation. From the experimental strain response it can be observed that first 60 sec the water is still and after 60sec current velocity increases rapidly until 130 sec. the water velocity is maintained constantly for about 100 sec and gradually to zero. Response estimation algorithm uses the same FE model used in numerical validation. The estimation consists of two steps. Step 1: estimate the input time history on each column with limited responses (Eq. 4.2), strain at unmeasured location is assumed to be same as nearest available strain response. Step 2: Calculate input covariance with available input time history and use limited response in Kalman filter based response estimation algorithm to estimate unmeasured responses. Overall estimation from Figure. 4.21 is in good agreement with measured responses. As it is difficult to see the dynamic component of estimation from Figure. 4.21, Figure. 4.22 shows the estimation between 130 and 140 sec.



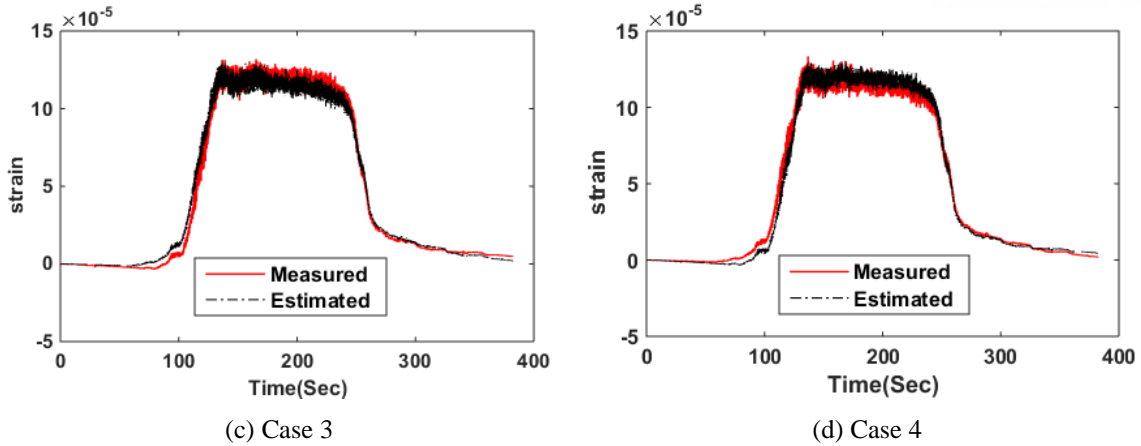


Figure. 4.21 Estimated and experimental strain response in time domain

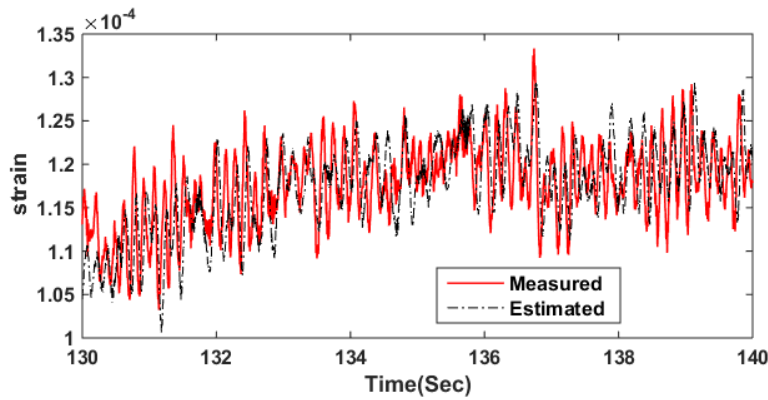


Figure. 4.22 Estimated and experimental strain response in column 4 (between 130 and 140 sec)

Unlike the reference strain from numerical model the strain data from experiment is subjected to small electrical noise (see Figure. 4.23), 60Hz peak can be observed. Where else in the estimated response the 60Hz peak is relatively smaller than the experimental response. The reason is multi-metric fusion of acceleration with strain helps to reduce the noise component from strain gauge.

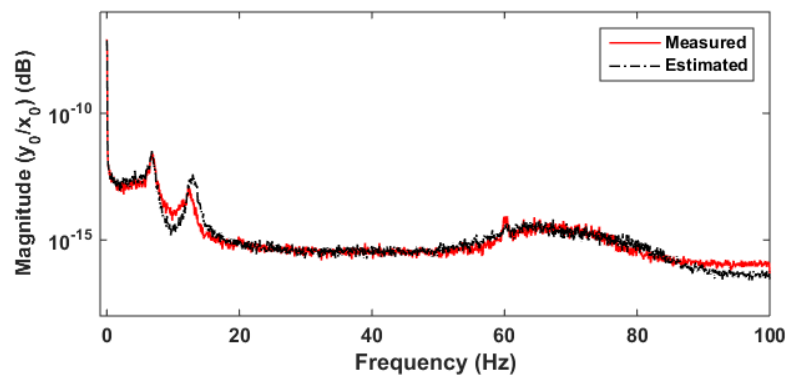


Figure. 4.23. Estimated and experimental strain response in frequency domain

Figure. 4.24 shows the RMSE error in estimated strain at each column. Strain estimation in Column 1 and 2 has higher error % which could arise based on strain deployment skills. The strain gauges should be deployed perpendicular to the plane of bending else the measured responses may not be accurate. Since the model and estimator assumes the strain measured are purely in x direction, the higher errors in column 1 and 2 could be due to improper sensor deployment. Column 3 and 4 has about 1% error.

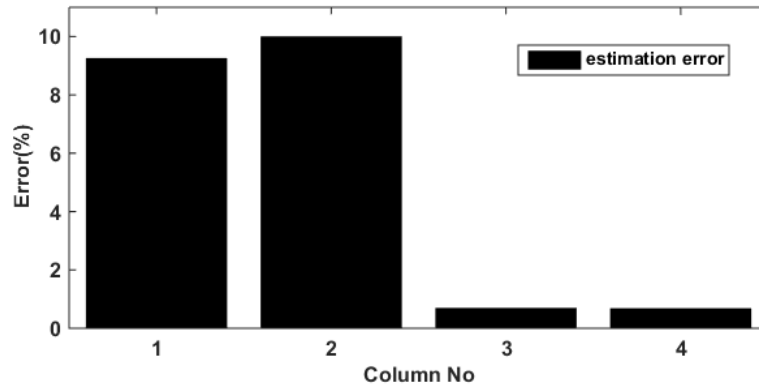


Fig. 4.24 Error in estimated strain at each column

Chapter 4

CONCLUSION, LIMITATION AND FUTURE SCOPE

The virtual sensing strategy tailored to SHM of offshore structures was proposed in this study. As the important structural members of the offshore structures are located under water, the virtual sensing strategy can be a powerful alternative to the direct measurement, particularly when the structural responses are desired at locations of unavailable sensors. The problem formulation for the virtual sensing based on the Kalman filtering was provided with how the non-zero mean input excitation can be properly handled for accurate response estimation. Different types of responses, viz., acceleration, tilt and strain, were employed as the input to Kalman filter. The strain and tilt response contributes to the low frequency, large amplitude trend in the estimation, while the acceleration with good high frequency information is capable of reducing the random noise. The numerical simulation was conducted with the finite element model of the small scale offshore structure. The non-stationary random input excitation varying depending on time and height is introduced to simulate the tidal current. The simulation result from offshore model showed that the estimation was accurate with errors all less than 1%. The laboratory experiment is subsequently conducted with the small scale offshore structure installed in the water channel. The virtual sensing strategy was shown to successfully find a strain response using the other three strains and the acceleration on the top plate. The numerical analysis and the experiment lead to the following conclusions:

- The redesigned Kalman state estimator has successfully estimated the strain responses at the unmeasured locations excited by the non-stationary random inputs in the numerical and experimental validation tests, even with the erroneous model used in the Kalman state estimator.
- The acceleration has been figured out to be improper to estimate the quasi-static trend of non-zero mean strain response excited by the non-zero mean input due to lack of accuracy in low frequency measurement near 0 Hz.
- The virtual sensing strategy has the potential to be able to capture structural responses of the bottom-fixed offshore structures under the non-stationary random tidal current.
- The fused use of the different types of measurements (i.e., strain and acceleration) can help to improve the estimation in lower and higher frequency regions.

This virtual sensing technique has general limitations and also under special conditions.

- When there is a damage at the location of estimation, the estimated response may not be accurate. If the damage can make a significant change in other measured sensors, in such a case estimation shall be accurate.
- The assumption of Gaussian distribution for random variables is also one of the limitation of this virtual sensing technique. Under some cases process noise distribution is not Gaussian.
- Since virtual sensing algorithm is executed at every timestamp, computationally overall SHM system becomes heavy and thus it needs a better processing hardware.

The virtual sensing strategy is seen to be quite useful for monitoring the offshore structures. Based on the findings in this dissertation, further study may include the use of the estimated response for the SHM purposes such as fatigue estimation and damage detection.

REFERENCES

1. Farrar, C. R., and Worken K., (2007), 'An introduction to structural health monitoring,' *Phil. Trans. R. Soc. A* (2007) **365**, 303–315 (doi:10.1098/rsta.2006.1928)
2. Iliopoulos, A.N., Devriendt, C., Iliopoulos, S.N. and Van Hemelrijck, D. (2014), "Continuous fatigue assessment of offshore wind turbines using a stress prediction technique", *Proc. of SPIE, Health Monitoring of Structural and Biological Systems 2014*, Vol. 9064 90640S-1, San Diego, California, USA, March.
3. Hjelm, H.P., Brincker, R., Graugaard-Jensen, J. and Munch, K. (2005), "Determination of stress histories in structures by natural input modal analysis", *Proceedings of the 23rd Conference and Exposition on Structural Dynamics (IMACXXIII)*, Orlando, Florida, USA, February
4. Yazid, E., Mohd, S.L., and Setyamartan, P. (2012), "Time-varying spectrum estimation of offshore structure response based on a time-varying autoregressive model", *J. Appl. Sci.*, **12(23)**, 2383-2389
5. Papadimitriou, C., Fritzen, C.P., Kraemer, P. and Ntotsios, E. (2009), "Fatigue lifetime estimation in structures using ambient vibration measurements", *Proceedings of the ECCOMAS Thematic Conference on Computational Methods in Structural Dynamics and Earthquake Engineering*, Rhodes, Greece, June.
6. Smyth, A. and Wu, M. (2007), "Multi-rate Kalman filtering for the data fusion of displacement and acceleration response measurements in dynamic system monitoring", *Mech. Syst. Signal Pr.*, **21(2)**, 706-723
7. Park, J.W., Sim, S.-H., and Jung, H.J. (2013), "Displacement estimation using multimetric data fusion", *IEEE T. Mech. - ASME.*, **18(6)**, 1675-1682
8. Soman, R.N., Onoufriou, T., Kyriakides, M.A., Votsis, R.A. and Chrysostomou, C.Z. (2014), "Multi-type, multi-sensor placement optimization for structural health monitoring of long span bridges", *Smart Struct. Syst.*, **14(1)**, 55-70
9. Park, J.W., Sim, S.-H. and Jung, H.J. (2014), "Wireless displacement sensing system for bridges using multi-sensor fusion", *Smart Mater. Struct.*, **23(4)**, 045022

10. Cho, S., Sim, S.-H., Park, J.W. and Lee, J. (2014), "Extension of indirect displacement estimation method using acceleration and strain to various types of beam structures", *Smart Struct. Syst.*, **14(4)**, 699-718
11. Jo, H., and Spencer, B.F. (2014), "Multi-Metric model based structure health monitoring", Proc. of SPIE, *Sensors and Smart Structures Technologies for Civil, Mechanical, and Aerospace Systems 2014*, San Diego, California, USA, March.
12. Van der Male, P. and Lourens, E. (2014), "Operational Vibration-Based Response Estimation for Offshore Wind Lattice Structures," *Proceedings of the International Modal Analysis Conference*.
13. Harrison R. L., 2010, 'Introduction To Monte Carlo Simulation', AIP Conf Proc. 2010 January 5; **1204**: 17–21. doi:10.1063/1.3295638.
14. Kalman, R.E. (1960), "A new approach to linear filtering and prediction problem," *Journal of Basic Engineering*, **82(1)**, 35-45.
15. G.L. Smith; S.F. Schmidt and L.A. McGee (1962). "Application of statistical filter theory to the optimal estimation of position and velocity on board a circumlunar vehicle". *National Aeronautics and Space Administration*.
16. Wan, E.A.; Van Der Merwe, R. (2000). "The unscented Kalman filter for nonlinear estimation". *Proceedings of the IEEE 2000 Adaptive Systems for Signal Processing, Communications, and Control Symposium (Cat. No.00EX373)*. p. **153**.
17. Park, J.W., Sim, S.-H. and Jung, H.J. (2014), "Wireless displacement sensing system for bridges using multi-sensor fusion", *Smart Mater. Struct.*, **23(4)**, 045022.
18. Smyth, A. and Wu, M. (2007), "Multi-rate Kalman filtering for the data fusion of displacement and acceleration response measurements in dynamic system monitoring", *Mech. Syst. Signal Pr.*, **21(2)**, 706-723.
19. Park, J.W., Sim, S.-H., and Jung, H.J. (2013), "Displacement estimation using multimetric data fusion", *IEEE T. Mech. - ASME.*, **18(6)**, 1675-1682.
20. Palanisamy, R. P., Cho, S., Kim, H., and Sim, S.-H. (2015), "Experimental validation of Kalman Filter-based strain estimation in structures subjected to non-zero mean input," *Smart Structures and Systems*, **15 (2)**, 489-503.

ACKNOWLEDGEMENT

I am using this opportunity to express my gratitude to everyone who supported me throughout the course of this dissertation.

I would like to express my deepest gratitude to my advisor, Dr. Sung-Han Sim, for his excellent guidance, caring, patience, and providing me with an excellent atmosphere for doing research. I would like to thank Dr. Jin-Hak Yi and Byung-Jin Jung who helped me to successfully validate the algorithm on offshore model. I would also like to thank my energetic colleagues Dr. Soojin Cho, Junhwa Lee, Eunjin Kim, Hyunjun Kim, Qandeel Hussain and Myunghwan Bae for their love and support throughout me research. My research would not have been possible without their helps.

Special thanks goes to Fritz Sihombing, Sreehari Prabhu, Junhwa Lee and Qandeel Hussain who are willing to help and give moral support throughout my stay in Korea. I would have been a lonely person without them.

Finally, I would like to thank my parents and elder sister. They were always supporting me and encouraging me with their best wishes.